

Compact, Large-Scale Photonic Neurons by Modulation-and-Weight Microring Resonators

Weipeng Zhang^{1,2,4*}, Yuxin Wang^{1,4}, Joshua C.
Lederman¹, Bhavin J. Shastri³ and Paul R. Prucnal^{1*}

^{1*}Department of Electrical and Computer Engineering, Princeton
University, Princeton, 08544, New Jersey, USA.

²LightXcelerate, Inc., Palo Alto, 94301, California, USA.

³Department of Physics, Engineering Physics and Astronomy,
Queen's University, Kingston, K7L 3N6, Ontario, Canada.

⁴The authors contribute equally to this paper.

*Corresponding author(s). E-mail(s): weipengz@princeton.edu;
prucnal@princeton.edu;

Contributing authors: yuxinw@princeton.edu;
joshuacl@princeton.edu; shastri@ieee.org;

Abstract

Fabrication imperfections, spatial constraints, and prohibitive costs collectively impede the scalability of neuromorphic photonics. In this work, we introduce a large-scale, compact photonic neuron in which each microring performs modulation and weighting simultaneously. This dual functionality is realized by leveraging both the carrier effect and thermal tunability, thereby merging modulation and weighting to conserve on-chip area, enhancing tuning efficiency, and capitalizing on wavelength-division multiplexing (WDM) for scalable implementations. In addition, we investigated a range of configurations for the proposed neuron to better tailor its behavior to various computational tasks. To illustrate the adaptability of the system's tasks, we explore both spatial and temporal domains, highlighting its versatility through two representative tasks: image processing and, for the first time, financial time series analysis, which represents a promising new frontier for neuromorphic photonics. These findings underscore the considerable promise of

photonic computing in addressing a breadth of real-world challenges, particularly under escalating demands for both scalability and flexibility.

Keywords: Silicon Photonics, Neuromorphic Photonics, Photonic Neuron Network

Introduction

Despite the promise of enhanced bandwidth, efficiency, and latency performance [1–4], neuromorphic photonic processors face ongoing challenges in achieving the practicality of their electronic counterparts [5, 6], largely due to significant scalability challenges [7]. As a result, photonic computing remains less effective in applications that involve large-scale AI models [8, 9] for complex data, such as text, graphics, and video. At the root of these scalability issues are device dimension constraints. Because the operational scale is dictated by the wavelength of light, photonic components cannot be arbitrarily miniaturized, thereby limiting the number of devices that can be integrated on a single chip. Moreover, even slight process variances introduced during fabrication can cause substantial performance discrepancies, making it difficult to maintain uniformity across nominally identical devices [10–13]. This is especially problematic for resonator-based elements, including microring resonators (MRRs) [14–16], which, despite their favorable compactness, are highly sensitive to fabrication inaccuracies.

A typical photonic processor requires consistent spectral alignment among its components, namely, the laser, modulator, weighting element, and photodetector [15, 17]. While the photodetector generally supports a broad wavelength range, aligning the other three components can be onerous, particularly because different MRRs often exhibit unpredictable, narrowly spaced resonant windows. Although a tunable laser can mitigate alignment issues for one MRR-based element, it becomes more complex when both the modulator and weighting element rely on MRRs that are not inherently matched. Such misalignment is not uncommon given the realities of manufacturing tolerances and environmental fluctuations [11, 14]. As the number of MRRs increases, these difficulties escalate exponentially, ultimately preventing the scaling of photonic processors.

To address these challenges, we propose a structurally novel neuron in which modulation and weighting are unified within a single MRR. By doing so, we reduce spectral alignment requirements to only two key components rather than three. Consequently, a tunable laser is sufficient for ensuring proper alignment, eliminating the added complexity of individually matching multiple MRR-based elements. To realize this approach, we leverage both thermal-optic and carrier effects in the same resonator, with additional merit of minimizing the overall footprint. We also found this modulation-and-weight

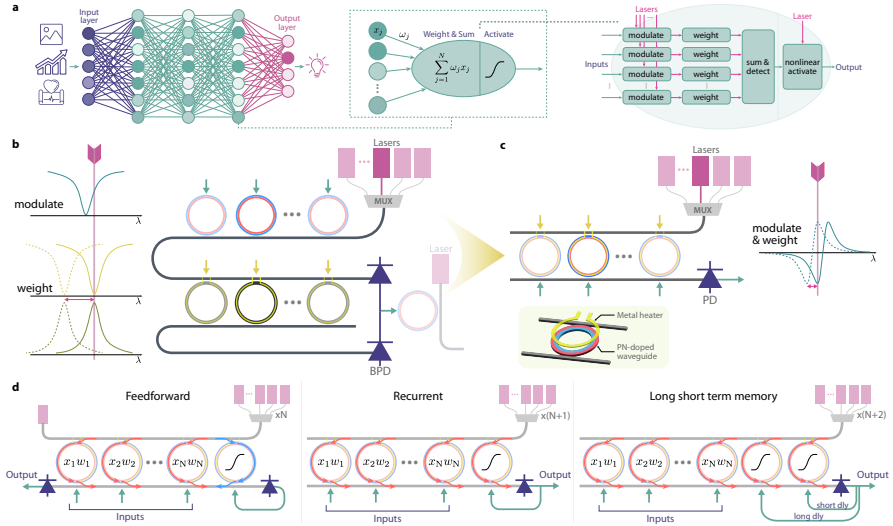


Fig. 1 (a) Neural network architecture composed of numerous small units that perform weighting, summation, and nonlinear activation. Photonic implementations typically require lasers and multiple integrated photonic devices for each of these functions. (b) A typical microring resonator (MRR)-based photonic neuron, comprising a bank of multiple lasers at different wavelengths, a ring modulator bank, an MRR-based weight bank, and a balanced photodetector. (c) The proposed approach, which consolidates both modulation and weighting in a single MRR bank and employs a single-ended photodetector, thereby reducing complexity and footprint. (d) Three possible configurations of the proposed MRR bank, enabling neuron types in feedforward, recurrent (short-term memory), and combined long/short-term memory modes.

MRR can be very efficient tuned as the transfer function between tuning current and weight becomes much steeper than conventional MRR for weighting only. Here, we present a major advancement in deploying this architecture at scale, demonstrated with a 10-MRR array configured in a 3×3 convolutional setup [18, 19] for image processing, including blurring, directional edge detection, and isotropic filtering, thereby showcasing the neuron’s ability to perform diverse spatial filtering operations. We also explore additional configurations that support feedforward and recurrent neuron models. Using all these configurations, we demonstrate the system’s applicability to time-series analysis by applying it to real-world stock price data, suggesting a potential opportunity for high-frequency financial analytics at near-light-speed latencies.

Results

Modulation-and-weight Microring Resonator

We implemented two tuning mechanisms to enable both modulation and weighting within a single MRR, which are: PN doping in the ring waveguide, which leverages carrier effects (carrier depletion and injection), and a metal heater on the ring, which provides thermal-optic tuning [16]. Both methods

modify the refractive index, thereby adjusting the optical power. Owing to its high bandwidth, the carrier effect is well-suited for modulating high-frequency input signals, whereas thermal tuning, though slower, offers a broader tuning range that is ideal for setting the bias point. Based on the small-signal model of the PN junction, when these mechanisms operate in tandem, the conversion efficiency—defined by the slope of the MRR transmission profile—varies substantially near the resonance peak. Consequently, only a small bias adjustment is required to shift the weight from its maximum positive to maximum negative setting, which translates into very tiny energy required for weight tuning. Moreover, integrating these two tuning approaches is fully compatible with standard silicon photonics foundry processes and is technically mature, requiring minimal additional refinement.

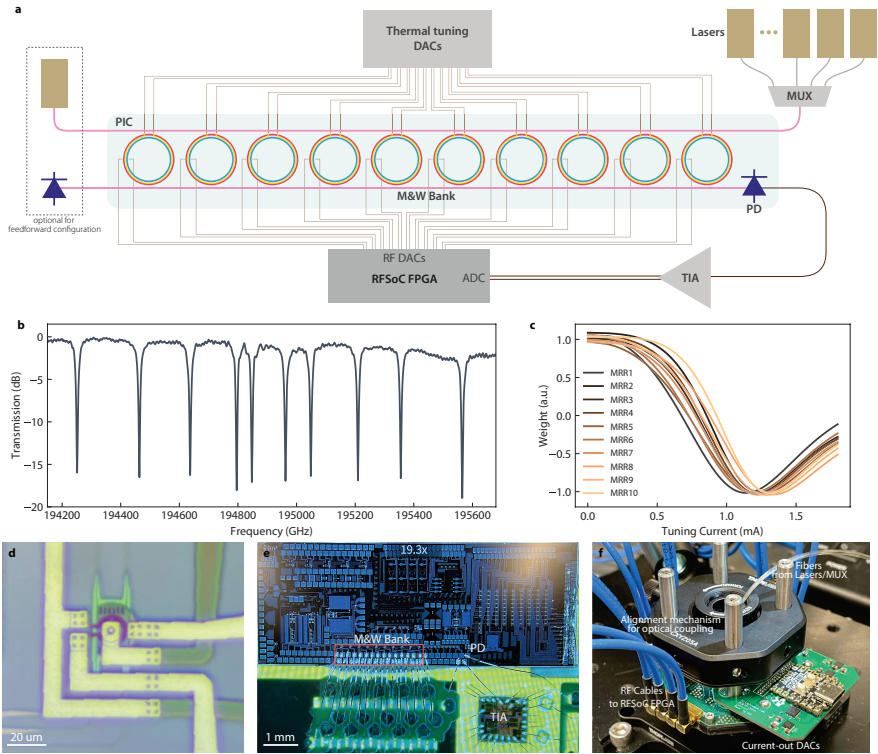


Fig. 2 Setup of this large-scale photonic processor. (a) System schematic. (b) Optical spectra. (c) Current-tuning curve of the ten MRRs. (d) Micrograph of the dual-modulation microring. (e) Micrograph of the photonic chip. (f) Photograph of the fully packaged chip.

As shown in Fig. 2(b), we fabricated a modulation-and-weight bank comprising ten MRRs. Each MRR has a slightly different radius, ranging from 8 to 8.10917 μm , resulting in a spectral spacing of approximately 12.12 nm between adjacent resonances (Fig. 2(c)). The chip was then fully packaged,

as illustrated in Fig. 2(b,e), by attaching an interposer printed circuit board (PCB) and wire-bonding all requisite pads. To drive the metal heater on each MRR, we integrated multi-channel current-output digital-to-analog converters, while impedance-controlled PCB traces provide the high-speed input signals for the PN junctions. The drop port of this modulation-and-weight bank is connected to a photodetector, which is wire-bonded to a transimpedance amplifier for signal readout. Regarding the energy consumption, figure 2(c) shows that all MRRs can tune across the range with just 1.3 mA of current, which translates to 0.55 mW, given the metal heaters have 330 Ohms of resistance. For comparison, conventional MRR for weighting typically consumes energy of 3 mW for the embedded metal heater (3mA, 330Ohms) and 1.5 mW for the doped waveguide heater (1.6mA, R=600 Ohms). Our architecture significantly reduces energy consumption compared to traditional designs with separated modulators and weighting elements, where thermal tuning can dominate the energy budget (up to 80%) [20]. Building on this improvement, the system also achieves a fully integrated photonic processor with a complete signal-processing path—from input modulation to output detection—thereby minimizing processing latency.

Compact and Configurable Photonic Neuron

The integration of modulation and weighting within a single MRR reduces the footprint, enabling more MRRs to be incorporated per neuron and thereby supporting a broader range of configurable architectures. The most common type, the feedforward neuron, performs weighted summation using only current inputs; after nonlinear activation, the output is propagated downstream. However, in many scenarios, performance improves by accounting for historical inputs. In our proposed photonic neuron, such a memory effect can be realized by re-routing the neuron output back to its input with a tunable delay. This approach is more straightforward in a large-scale neuron that has sufficient MRRs available. With ten MRRs available, a selected subset can process real-time inputs, while the rest handle recurrent (historical) data. As illustrated in Fig. 1(d), we present two such recurrent implementations, using one or two MRRs for past data. By adjusting the length of the electrical path from the photodetector output to the MRR input, we can fine-tune the delay and thereby accommodate both short- and long-term memory effects. This flexibility is especially advantageous for time-series data, such as electrocardiogram (ECG) [21] or radio-frequency (RF) signals [2, 22, 23], where crucial hidden features may only emerge when both current and previous inputs are considered. In the following sections, we first evaluate the proposed neuron in a convolutional image task that processes only recent inputs, and subsequently demonstrate the benefits of its memory capability in a financial time-series context.

Demonstration on Image Processing

To evaluate the image processing capability of the system, we configured 9 of the 10 MRRs into a 3×3 convolutional kernel. We utilized a field-programmable gate array (FPGA, Xilinx RFSoc series) board with built-in digital-to-analog converters (DACs) to generate image signals. Regarding the convolutional processing, each original image data was flattened, converting it from a two-dimensional array to a one-dimensional sequence. Each MRR receives a time-shifted version of the image signal corresponding to a specific pixel within the 3×3 convolution window, implemented through staggered DAC output (Fig. 3 a). The time offsets are calculated based on relative pixel positions, with horizontal and vertical shifts determined by image dimensions (64×64 in this test).

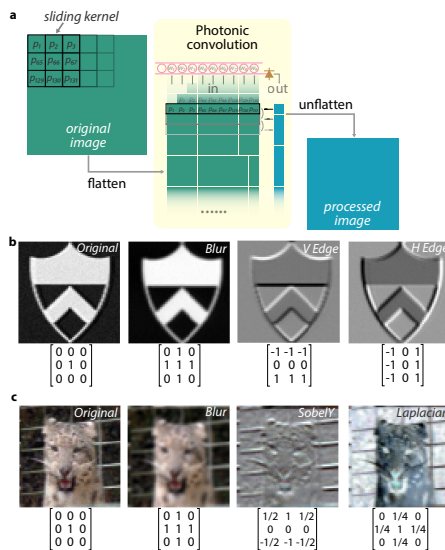


Fig. 3 (a) Schematic illustration of photonic image convolution. (b) Grayscale and (c) color image outputs produced by convolving each original image (leftmost in each row) with three different kernels, whose values are indicated in the top-right corner of each processed image. In addition to the blurring effect—achieved by averaging neighboring pixels—other kernels highlight edge detection by computing local derivatives in specific directions. The Laplacian kernel applies an isotropic derivative, enhancing high-frequency features, such as the thin vertical and horizontal lines of the fence behind the tiger.

Test images with a resolution of 64×64 pixels (4096 points/channel) are serialized and shaped by a raised-cosine filter (roll-off = 0.35), with each symbol represented by 16 samples to mitigate inter-symbol interference. The digital-to-analog converters (DACs) operate at 9.8304 GSPS, delivering an effective data rate of approximately 820 MHz. The ten MRRs span a spectral window from 194200 GHz to 195600 GHz, facilitating standard wavelength-division multiplexing (WDM) with ten tunable lasers combined into a single

fiber for coupling into the chip. Once the system is aligned, each laser’s tuning curve is measured, demonstrating classic kernels for edge detection, Sobel filtering, and Gaussian blurring. The resulting outputs exhibit visually accurate edge maps and blurred images that closely match digital references, confirming the system’s capability to implement spatial filtering optically.

Moreover, this setup exhibits very low latency, a small footprint, and modest energy consumption. The modulator and photodetector are integrated on the same chip, linked by a 4 mm waveguide; consequently, the effective processing latency—determined by the light’s travel time—is on the order of tens of picoseconds. Utilizing a single MRR for dual-function reduces the chip area per input channel to 0.165 mm^{-2} , inclusive of bonding pads and traces. As shown in Fig. 2(d), all MRRs can be tuned over the required range with just 1.3 mA of current, equating to 0.55 mW given the 330 Ohms resistance of the metal heaters. These compact footprint and low-power characteristics confirm the viability of this photonic processing architecture. Furthermore, compatibility with WDM allows the inclusion of additional MRRs with distinct resonances, accommodating up to 30 channels based on the current free spectral range and resonance width of each MRR. In short, our proposed architecture addresses scalability and alignment challenges in photonic processing by integrating modulation and weighting in a single MRR. The successful implementation of image processing tasks validates its practical potential, and we anticipate that this large-scale approach will significantly expand the applicability of neuromorphic photonic processors, particularly in handling high-frequency time-series signals.

Simulation on High Frequency Trading

As demonstrated in the previous section, the inherently high throughput of our photonic processor—realized with just ten MRRs—demonstrates its strong capability for large-scale data processing using a convolutional configuration. In this section, we further enhance the proposed photonic neuron by incorporating nonlinear functionality, enabling more complex data processing with improved intelligence. Among potential real-world applications, neuromorphic photonics emerges as an ideal candidate for high-frequency trading (HFT), given its need for rapid analysis of extensive historical financial data and low-latency decision-making. Despite its obvious potential, this domain has rarely—or perhaps never—been addressed via photonic solutions.

High-frequency trading, unlike traditional portfolio management, aims to execute numerous trades in quick succession, thereby accumulating small gains that collectively result in significant profits. A well-known principle in HFT is the advantage secured by those who can make faster, high-quality decisions. In fact, the speed of light is so critical in HFT that optical fiber links are commonly deployed between trading firms and exchanges. However, before the advent of photonic processors, the state-of-the-art HFT systems relied on field-programmable gate arrays (FPGAs), which offer the lowest latency currently

achievable in electronics but remain constrained by clock-speed limits that usually bottlenecked at few GHz.

Here, we demonstrate that a single photonic neuron can be configured to serve as a high-frequency trading (HFT) mechanism with dramatically reduced latency. As depicted in Fig. 1(d), the neuron is reconfigured in a recurrent manner, using nine MRRs for input signals and one additional MRR dedicated to nonlinearity and historical feedback.

We evaluate the proposed system on three S&P 500 stocks—AAPL, TSLA, and GOOG—using price data at 1 s intervals for the past 20 trading days, the highest temporal resolution offered by the chosen data source (Yahoo Finance). At each step, ten consecutive data points are streamed to the MRRs via the FPGA at a sampling rate of 1 GSPS. For each stock, the first 14 trading days are utilized for training, and the most recent 6 days are reserved for testing. Because the high-speed input/output interfaces of the photonic neuron are directly connected to an RFSoc FPGA that also computes trading performance via its on-board processor, we can employ online (in-situ) training to optimize the tuning currents (weights) of all ten MRRs in real-time. The optimization is performed using a particle swarm optimization [24] (PSO) algorithm, which does not require gradient calculations and converges relatively quickly in the 11-dimensional parameter space (10 MRR currents plus one bias). As discussed previously, this in-situ training effectively compensates for environmental drifts that may shift ring resonances, thus preserving optimal performance.

Performance results for the photonic HFT system are presented in Fig. 4. The photodetector output from the recurrent network is digitized and thresholded by the FPGA to yield discrete trading decisions—buy, sell, or watch—as indicated by the symbols in the middle row of Fig. 4. The insets in this row illustrate the final weights of the ten MRRs trained for each stock, showing how the photonic neuron converges to configurations tailored to the unique characteristics of different equities. This adaptability ultimately produces robust gains, reflected by the steadily increasing profit curves shown in the bottom row.

As illustrated in Fig. 1(d), the proposed modulate-and-weight neuron accommodates a range of configurations that extend beyond convolving the 10 most recent inputs. In particular, it allows short- or long-term memory via a recurrent arrangement—a feature especially beneficial for high-frequency trading tasks, where historical data may provide insights not captured by the most recent observations alone. Consequently, we evaluated our single photonic neuron under three distinct configurations for the AAPL stock symbol, as presented in Fig. 5.

The charts on the left depict performance over 20 consecutive trading days, with the training and testing intervals shown in blue and orange, respectively. Although there is no guarantee of net gains on every single day, the incorporation of historical data clearly enhances robustness, as evidenced by reduced variability and higher gain-to-loss ratios. The charts on the right illustrate

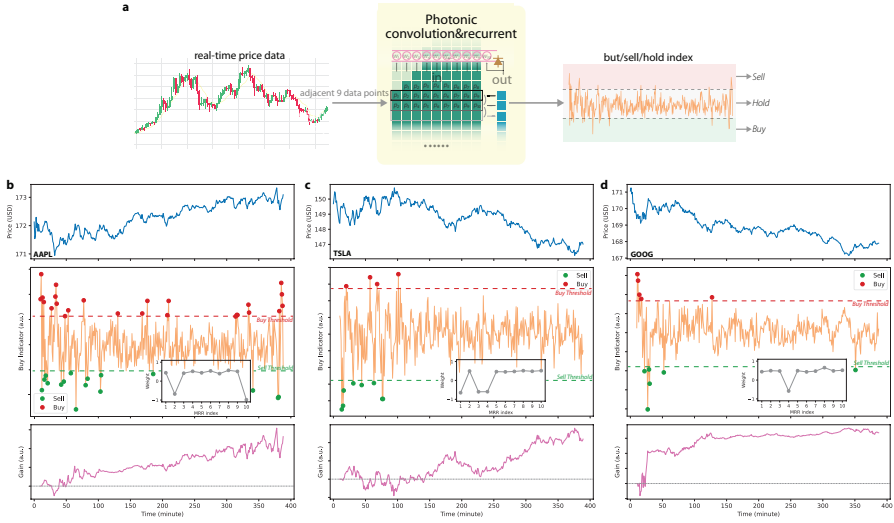


Fig. 4 Results of high-frequency trading. (a)–(c) correspond to three different stock symbols—AAPL, TSLA, and GOOG, respectively. In each panel, the top row shows the stock price over one trading day. The middle row displays the photonic neuron output, generated by convolving 10 consecutive price points; green and red dots denote sell and buy signals, respectively. The bottom row illustrates the resulting profit, demonstrating robust gains for all tested stocks, regardless of whether their daily price trended upward or downward.

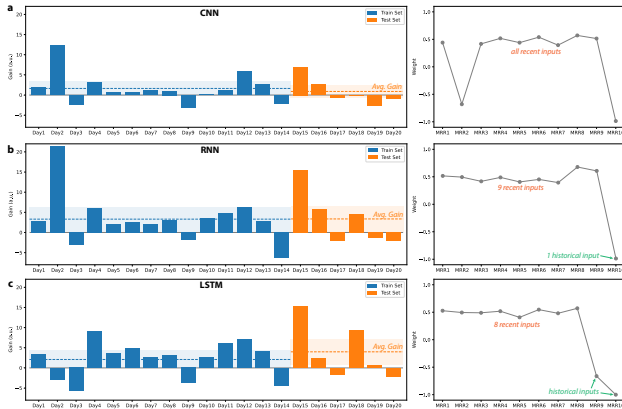


Fig. 5 Performance comparison of the photonic HFT using three different neuron type, which are (a) basic convolution, (b) convolution with one historical recurrent, and (b) convolution with two historical recurrensts with short and long delays.

the trained weights for each configuration. In all cases, the neuron effectively computes the derivative of the stock price—a strategy that intuitively facilitates trade-signal detection by identifying shifts in price. Among the three configurations, the convolutional neural network (CNN) approach focuses on both the most recent and the oldest price derivatives, as indicated by negative

weights on MRRs 2 and 10. By contrast, the other two configurations leverage historical feedback, tending to average recent data while comparing it to past values, signaled by negative weights on the final one or two MRRs. These observations underscore the versatility and emergent intelligence of the proposed photonic neuron, even when demonstrated at the relatively small scale of a single neuron.

Note that the current demonstration serves only as a simplified model of high-frequency trading (HFT), where optimal trading opportunities often arise on the order of a few nanoseconds. This ultrafast timescale explains why field-programmable gate arrays (FPGAs) remain dominant in HFT, achieving latencies in the few-hundred-nanosecond range. Furthermore, the advent of Internet and electronic computing has already revolutionized the original bulletin-board trading system. As neuromorphic photonic processors mature—encompassing larger computational scales and more sophisticated nonlinearities, as demonstrated in this work—we envision a new paradigm. This paradigm would capture price data immediately after it traverses optical fibers, eliminating the need for conventional Ethernet access and electronic processors, and ultimately delivering the ultra-low latencies demanded by HFT.

Conclusion

In conclusion, we introduce a large-scale, compact, and versatile photonic neuron implementation that tackles the spectral alignment challenge through a unified modulation-and-weight MRR bank architecture. Using a single neuron composed of ten MRRs, we validated its efficacy on a classic image-processing task and demonstrated its potential in a novel real-world domain—high-frequency trading.

By consolidating modulation and weighting within the same resonator, spectral alignment is substantially simplified, enabling a straightforward 10 MRR configuration. The system versatility is further enhanced by its configurability; beyond the standard feedforward approach, any subset of MRRs can handle linear weighted summation while the remainder provides nonlinear activation with adjustable delays. We anticipate that this newly enhanced photonic neuron architecture will serve as a scalable building block for future neuromorphic photonic systems, designed to handle large-scale and complex tasks across an expanding range of real-world applications.

Methods

Photonic chip packaging

The photonic integrated circuit (PIC), along with two transimpedance amplifiers (TIAs) and several decoupling capacitors, is mounted directly onto the top printed circuit board (PCB) using silver epoxy and wire-bonded to the PCB pads for electrical interconnects. Rogers 4003C serves as the PCB substrate to

accommodate high-frequency signals with minimal loss. Radio-frequency (RF) signals enter and exit the PCB via SMP connectors and traverse impedance-controlled traces to the PIC. Optical coupling is accomplished through a glued fiber array, polished at a 41° angle to match the on-chip grating couplers at 8° , yielding a measured coupling loss of approximately 7 dB per fiber-to-chip pass.

A ribbon cable links the top PCB to a bottom PCB, which supplies tuning currents for the MRR weight banks and bias voltages for the MRR modulators and balanced photodetectors (BPDs). This bottom PCB is populated with two 5-channel current-output DACs (LTC2662, Analog Devices) and one 8-channel voltage DAC (LTC2686, Analog Devices), along with several low-noise linear power modules to generate the required +5 V, +10 V, and -10 V rails. The bottom PCB also interfaces with the FPGA board via a high-speed SPI link for configuration and control. Additionally, a thermoelectric cooler is located between the two PCBs, working in conjunction with a thermistor on the top board and a dedicated temperature controller to maintain thermal stability.

Compact optical coupling

Optical coupling requires precise alignment between the external fiber array and the on-chip grating couplers. This process involves a trade-off between permanent solutions (e.g., epoxy bonding, photonic wire bonding), which lack replaceability, and bulky temporary setups (e.g., multi-axis alignment stages), which can be cumbersome. To address this challenge, we developed a compact alignment mechanism for temporary optical packaging that is compatible with grating couplers. Our design employs a Thorlabs optical cage system consisting of two primary mounting plates connected by four rods. The interposer PCB carrying the photonic chip is affixed to the bottom plate (Thorlabs CXYZ05A), enabling rotation about the z-axis. The fiber array is secured to the top plate (Thorlabs CRM1PT) via a custom adapter, providing translational movement in the x, y, and z directions. The adapter features an inclined mounting plane set at 37° to the x–y plane, matching the angle required by the grating couplers.

Using an on-chip loop waveguide that routes one grating coupler directly to another, we measured a round-trip loss of approximately 11 dB and observed a long-term drift of less than 0.05 dB. Accounting for the inherent waveguide losses, this corresponds to a coupling efficiency better than 5.5 dB—comparable to bulkier setups with more sophisticated alignment mechanisms [14].

FPGA-based Signal Generation

The FPGA board used in this setup is a Xilinx RFSoc series model that provides a multi-channel, high-speed, and cost-effective solution for both signal generation (digital-to-analog conversion) and signal digitization (analog-to-digital conversion). Specifically, we employed the HTG-ZRF16 board from HiTech Global, featuring a ZU49DR RFSoc FPGA chip. This board can be programmed using either Xilinx’s official Vivado software or the third-party

CasperFPGA firmware, developed by the Collaboration for Astronomy Signal Processing and Electronics Research (CASPER), a consortium of multiple research groups. The FPGA program utilized in this work was derived from CasperFPGA, and we gratefully acknowledge the CASPER organization for making their code openly available.

Data Availability

All data used in this study are available from the corresponding authors upon request.

Code Availability

All codes used in this study are available from the corresponding authors upon request.

References

- [1] Brunner, D., Shastri, B.J., Qadasi, M.A.A., Ballani, H., Barbay, S., Biasi, S., Bienstman, P., Bilodeau, S., Bogaerts, W., Böhm, F., et al.: Roadmap on neuromorphic photonics. arXiv preprint arXiv:2501.07917 (2025)
- [2] Zhang, W., Lederman, J.C., Ferreira de Lima, T., Zhang, J., Bilodeau, S., Hudson, L., Tait, A., Shastri, B.J., Prucnal, P.R.: A system-on-chip microwave photonic processor solves dynamic rf interference in real time with picosecond latency. *Light: Science & Applications* **13**(1), 14 (2024)
- [3] Shekhar, S., Bogaerts, W., Chrostowski, L., Bowers, J.E., Hochberg, M., Soref, R., Shastri, B.J.: Roadmapping the next generation of silicon photonics. *Nature Communications* **15**(1), 751 (2024)
- [4] Huang, C., Sorger, V.J., Miscuglio, M., Al-Qadasi, M., Mukherjee, A., Lampe, L., Nichols, M., Tait, A.N., Ferreira de Lima, T., Marquez, B.A., et al.: Prospects and applications of photonic neural networks. *Advances in Physics: X* **7**(1), 1981155 (2022)
- [5] Wang, Y.E., Wei, G.-Y., Brooks, D.: Benchmarking tpu, gpu, and cpu platforms for deep learning. arXiv preprint arXiv:1907.10701 (2019)
- [6] Reuther, A., Michaleas, P., Jones, M., Gadepally, V., Samsi, S., Kepner, J.: Survey and benchmarking of machine learning accelerators. In: 2019 IEEE High Performance Extreme Computing Conference (HPEC), pp. 1–9 (2019). IEEE
- [7] Xu, X.-Y., Jin, X.-M.: Integrated photonic computing beyond the von neumann architecture. *ACS Photonics* **10**(4), 1027–1036 (2023)

- [8] Vaswani, A.: Attention is all you need. *Advances in Neural Information Processing Systems* (2017)
- [9] Kaplan, J., McCandlish, S., Henighan, T., Brown, T.B., Chess, B., Child, R., Gray, S., Radford, A., Wu, J., Amodei, D.: Scaling laws for neural language models. *arXiv preprint arXiv:2001.08361* (2020)
- [10] Xu, T., Zhang, W., Zhang, J., Luo, Z., Xiao, Q., Wang, B., Luo, M., Xu, X., Shastri, B.J., Prucnal, P.R., *et al.*: Control-free and efficient integrated photonic neural networks via hardware-aware training? and pruning. *Optica* **11**(8), 1039–1049 (2024)
- [11] Ferreira de Lima, T., Doris, E.A., Bilodeau, S., Zhang, W., Jha, A., Peng, H.-T., Blow, E.C., Huang, C., Tait, A.N., Shastri, B.J., *et al.*: Design automation of photonic resonator weights. *Nanophotonics* **11**(17), 3805–3822 (2022)
- [12] Bogaerts, W., Chrostowski, L.: Silicon photonics circuit design: methods, tools and challenges. *Laser & Photonics Reviews* **12**(4), 1700237 (2018)
- [13] Bogaerts, W., Fiers, M., Dumon, P.: Design challenges in silicon photonics. *IEEE Journal of Selected Topics in Quantum Electronics* **20**(4), 1–8 (2013)
- [14] Zhang, W., Huang, C., Peng, H.-T., Bilodeau, S., Jha, A., Blow, E., Ferreira de Lima, T., Shastri, B.J., Prucnal, P.: Silicon microring synapses enable photonic deep learning beyond 9-bit precision. *Optica* **9**(5), 579–584 (2022)
- [15] Tait, A.N., Wu, A.X., Ferreira de Lima, T., Zhou, E., Shastri, B.J., Nahmias, M.A., Prucnal, P.R.: Microring weight banks. *IEEE Journal of Selected Topics in Quantum Electronics* **22**(6), 312–325 (2016)
- [16] Bogaerts, W., De Heyn, P., Van Vaerenbergh, T., De Vos, K., Kumar Selvaraja, S., Claes, T., Dumon, P., Bienstman, P., Van Thourhout, D., Baets, R.: Silicon microring resonators. *Laser & Photonics Reviews* **6**(1), 47–73 (2012)
- [17] Huang, C., Bilodeau, S., Ferreira de Lima, T., Tait, A.N., Ma, P.Y., Blow, E.C., Jha, A., Peng, H.-T., Shastri, B.J., Prucnal, P.R.: Demonstration of scalable microring weight bank control for large-scale photonic integrated circuits. *APL Photonics* **5**(4) (2020)
- [18] Li, Z., Liu, F., Yang, W., Peng, S., Zhou, J.: A survey of convolutional neural networks: analysis, applications, and prospects. *IEEE transactions on neural networks and learning systems* **33**(12), 6999–7019 (2021)

- [19] Xu, X., Tan, M., Corcoran, B., Wu, J., Boes, A., Nguyen, T.G., Chu, S.T., Little, B.E., Hicks, D.G., Morandotti, R., *et al.*: 11 tops photonic convolutional accelerator for optical neural networks. *Nature* **589**(7840), 44–51 (2021)
- [20] Narayana, V.K., Sun, S., Badawy, A.-H.A., Sorger, V.J., El-Ghazawi, T.: Morphonoc: Exploring the design space of a configurable hybrid noc using nanophotonics. *Microprocessors and Microsystems* **50**, 113–126 (2017)
- [21] Dong, B., Aggarwal, S., Zhou, W., Ali, U.E., Farmakidis, N., Lee, J.S., He, Y., Li, X., Kwong, D.-L., Wright, C., *et al.*: Higher-dimensional processing using a photonic tensor core with continuous-time data. *Nature Photonics* **17**(12), 1080–1088 (2023)
- [22] Lederman, J.C., Zhang, W., de Lima, T.F., Blow, E.C., Bilodeau, S., Shastri, B.J., Prucnal, P.R.: Real-time photonic blind interference cancellation. *Nature communications* **14**(1), 8197 (2023)
- [23] Zhang, W., Tait, A., Huang, C., Ferreira de Lima, T., Bilodeau, S., Blow, E.C., Jha, A., Shastri, B.J., Prucnal, P.: Broadband physical layer cognitive radio with an integrated photonic processor for blind source separation. *Nature communications* **14**(1), 1107 (2023)
- [24] Kennedy, J., Eberhart, R.: Particle swarm optimization. In: *Proceedings of ICNN'95-international Conference on Neural Networks*, vol. 4, pp. 1942–1948 (1995). *ieee*

Acknowledgments

This research is supported by the National Science Foundation (NSF) (ECCS-2128616 and ECCS-1642962 to P.R.P.), the Office of Naval Research (ONR) (N00014-18-1-2297 and N00014-20-1-2664 P.R.P.), and the Defense Advanced Research Projects Agency (HR00111990049 to P.R.P.). The devices were fabricated at the Advanced Micro Foundry (AMF) in Singapore through the support of CMC Microsystems. B. J. Shastri acknowledges support from the Natural Sciences and Engineering Research Council of Canada (NSERC).

Author contributions

W.Z. conceived the ideas. W.Z. and Y.W. designed the experiment and conducted the experimental measurements. W.Z. analyzed the results. J.C.L. designed the silicon photonic chip. B.J.S. provided theoretical support. W.Z., and B.J.S. wrote the manuscript. P.R.P. supervised the research and contributed to the general concept and interpretation of the results. All the authors discussed the data and contributed to the manuscript.

Competing interests

The authors declare no competing interests.